Colloids and Surfaces B: Biointerfaces 132 (2015) 71–77

Contents lists available at ScienceDirect

Colloids and Surfaces B: Biointerfaces

journal homepage: www.elsevier.com/locate/colsurfb

Unaffected features of BSA stabilized Ag nanoparticles after storage and reconstitution in biological relevant media

Laura E. Valenti[a,b], Carla E. Giacomelli[a,*]

[a] Instituto de Investigaciones en Físico Química de Córdoba (INFIQC) CONICET-UNC, Departamento de Fisicoquímica, Facultad de Ciencias Químicas, Universidad Nacional de Córdoba, Ciudad Universitaria, Córdoba X5000HUA, Argentina
[b] Raomed S. A., Av. Circunvalación 3085, Córdoba X5011CTR, Argentina

ARTICLE INFO

Article history:
Received 25 February 2015
Received in revised form 20 April 2015
Accepted 6 May 2015
Available online 14 May 2015

Keywords:
Bovine serum albumin
Silver nanoparticle
Stabilization mechanism
Colloidal stability
Antimicrobial activity
Freeze dry

ABSTRACT

Silver-coated orthopedic implants and silver composite materials have been proposed to produce local biocidal activity at low dose to reduce post-surgery infection that remains one of the major contributions to the patient morbidity. This work presents the synthesis combined with the characterization, colloidal stability in biological relevant media, antimicrobial activity and handling properties of silver nanoparticles (Ag-NP) before and after freeze dry and storage. The nanomaterial was synthesized in aqueous solution with simple, reproducible and low-cost strategies using bovine serum albumin (BSA) as the stabilizing agent. Ag-NP were characterized by means of the size distribution and morphology (UV–vis spectra, dynamic light scattering measurements and TEM images), charge as a function of the pH (zeta potential measurements) and colloidal stability in biological relevant media (UV–vis spectra and dynamic light scattering measurements). Further, the interactions between the protein and Ag-NP were evaluated by surface enhanced Raman spectroscopy (SERS) and the antimicrobial activity was tested with two bacteria strains (namely *Staphylococcus aureus* and *Staphylococcus epidermidis*) mainly present in the infections caused by implants and prosthesis in orthopedic surgery. Finally, the Ag-NP dispersed in aqueous solution were dried and stored as long-lasting powders that were easily reconstituted without losing their stability and antimicrobial properties. The proposed methods to stabilize Ag-NP not only produce stable dispersions in media of biological relevance but also long-lasting powders with optimal antimicrobial activity in the nanomolar range. This level is much lower than the cytotoxicity determined *in vitro* on osteoblasts, osteoclasts and osteoarthritic chondrocytes. The synthesized Ag-NP can be incorporated as additive of biomaterials or pharmaceutical products to confer antimicrobial activity in a powdered form in different formulations, dispersed in aqueous and non-aqueous solutions or coated on the surface of different materials.

1. Introduction

Numerous methods have been reported for the synthesis of silver nanoparticles (Ag-NP) [1,2] mainly due to their broad antimicrobial properties and potential anticancer applications [3]. Ag-NP offer many distinctive advantages in reducing acute toxicity, overcoming resistance, and lowering cost, when compared to conventional antibiotics [4]. Nowadays, implant infection remains one of the most serious complications in orthopedic surgery with a major contribution to the patient morbidity [5]. These types of complications account for more than half of all hospital acquired infections and are the most complex and costly to treat. In order to reduce post-surgery infections, silver-coated orthopedic implants [6,7] and silver composite materials [8] have been proposed to produce local biocidal activity at low dose [9].

Considering that human exposure to foreign materials inevitable raises concerns on new health risks, Ag-NP have been also the subject of extensive nanotoxicology studies using *in vivo* and *in vitro* experiments [10–12]. The outcome is still limited and somewhat contradictory, especially because the size, shape and surface properties of Ag-NP strongly affect the antimicrobial activity *versus* cytotoxicity response [13]. In addition, the toxic concentration varies greatly from different mammalian cells as well as the inhibitory concentration changes for different bacteria strains. In general, a significant dose-dependent effect has been observed; clearly indicating that high efficacy at the lowest possible concentration is a major requirement of antimicrobial NP-Ag to be used in orthopedic related biomaterials [10,11].

* Corresponding author. Tel.: +54 3515353866; fax: +54 3514334188.
E-mail address: giacomel@fcq.unc.edu.ar (C.E. Giacomelli).

http://dx.doi.org/10.1016/j.colsurfb.2015.05.002
0927-7765/

Due to the large positive reduction potential of Ag^+ ions, Ag-NP oxidation is thermodynamically unfavorable resulting in quite stable aqueous suspensions without the aid of capping ligands. However, biological relevant media strongly induce Ag-NP aggregation due to the high ionic strength that reduces the electrical double layer around the NP [14]. Therefore, capping agents such as self-assembled monolayers [15], surfactants [16], polymers [17], dendrimers [18] and proteins [19–21] have been employed to protect Ag-NP from aggregation. Protein molecules not only are excellent stabilizing agent but also create biofunctionalized Ag-NP [22–25]. Biofunctionalization is very important to achieve biocompatibility, which is one of the primary criteria to use Ag-NP in orthopedic implants. Further, NP adhesion to the surface of biomaterials may be improved by protein mediated interactions [26]. Finally, a critical but often overlooked drawback of Ag-NP suspensions involves their short- and long-term storage due to oxidation and photoassisted reactions [27,28]. Hence, it is necessary to prepare long-lasting Ag-NP in terms of size, shape and physicochemical properties to formulate new types of safe and cost-effective biocidal agents.

This work presents the synthesis combined with the characterization, colloidal stability in biological relevant media, antimicrobial activity and handling properties of Ag-NP before and after freeze dry and storage. The nanomaterial was synthesized in aqueous solution with simple, reproducible and low-cost strategies using bovine serum albumin (BSA) as the stabilizing agent. Albumin is a versatile protein for NP biofunctionalization, which is non-toxic, biocompatible and biodegradable [23,24,29]. Ag-NP were characterized by means of the size distribution and morphology (UV–vis spectra, dynamic light scattering measurements and TEM images), charge as a function of the pH (zeta potential measurements) and colloidal stability in biological relevant media (UV–vis spectra and dynamic light scattering measurements). Further, the interactions between the protein and Ag-NP were evaluated by surface enhanced Raman spectroscopy (SERS) and the antimicrobial activity was tested with two bacteria strains (namely *Staphylococcus aureus* and *Staphylococcus epidermidis*) mainly present in the infections caused by implants and prosthesis in orthopedic surgery. Finally, the Ag-NP dispersed in aqueous solution were dried and stored as long-lasting powders that were easily reconstituted without losing their stability and antimicrobial properties.

2. Experimental

2.1. Material

$AgNO_3$ were obtained from Carlo Erba, $NaBH_4$ from Tetrahedron, BSA from Sigma, the Mueller Hinton Broth (MHB) and Agar from Britania and trisodium citrate, $NaNO_3$ and K_2HPO_4 from J. T. Baker. All reagents were of analytical grade and used without further purification.

Aqueous solutions were prepared in deionized water (Milli Q System, Millipore). The pH adjustment were performed by adding NaOH or HNO_3 solutions and the pH measurements carried out with a glass electrode and a digital pH meter (Mettler Toledo – Seven Compact). All experiments were performed at room temperature ($25 \pm 2\,^{\circ}C$) unless otherwise stated.

2.1.1. Bacterial strains

S. aureus (ATCC 29213) and *S. epidermidis* (ATCC 12228) were kindly provided by Dr. Claudia Sola (CIBICI-CONICET, Universidad Nacional de Córdoba, Córdoba, Argentina) and Dr. Paola Ceriana (INEI ANLIS Instituto Malbran, Buenos Aires, Argentina), respectively.

2.2. Methods

2.2.1. Synthesis of Ag-NP

Ag-NP (Ag-NP/citrate) samples were synthesized following the procedure described by Lok et al. [30] with some modifications. Briefly, 1 mL of 0.1 mol L^{-1} $AgNO_3$ was added with vigorously stirring to 100 mL of 7×10^{-4} mol L^{-1} trisodium citrate solution. Afterwards, the reduction step was performed with 1 mL of 0.13 mol L^{-1} $NaBH_4$ which was added slowly. The resulting suspension was stirred until no changes in the color were observed. BSA was incorporated in two different stages of the Ag-NP synthesis: after (Ag-NP/BSA1) and before (Ag-NP/BSA2) the reduction of Ag^+ ions. In the first case, 10 mL of 1% (w/v) of BSA solution in 0.05 mol L^{-1} phosphate buffer pH 8.0 were added to the as prepared Ag-NP/citrate dispersion. In the second one, 10 mL of BSA solution (1%, w/v in 0.05 mol L^{-1} phosphate buffer pH 8.0) were added to the reaction medium before the reduction step by $NaBH_4$. Finally, Ag-NP/BSA1 and Ag-NP/BSA2 were freeze-dried over a 24 h period.

Powdered Ag-NP/BSA2 were added to the solid component of either bone cement (Simplex P – Stryker) or bone substitute (Hydroset – Stryker) to prepare the corresponding biomaterials using the nanoparticles at a ratio of 5% of the solid components of the samples. The samples were prepared following the indications of the manufacturer using 1 g of the solid component to obtain 8 cylindrical samples of 6 mm diameter and 3 mm height. The release amount of Ag-NP was calculated from the concentration of Ag^+ ions potentiometrically determined assuming that ions were released from spherical 4 nm nanoparticles.

2.2.2. UV–vis spectroscopic measurements of Ag-NP samples

UV–vis spectra were obtained in the 320–800 nm range using a UV-1700 PharmaSpec Shimadzu spectrophotometer at a spectral resolution of 0.5 nm. All Ag-NP samples were diluted twenty times with deionized water before collecting.

2.2.3. Transmission electron microscopy (TEM)

Imaging of Ag-NP was performed by using a JEOL EXII Transmission Electron Microscope. Aliquots of sonicated Ag-NP dispersions were placed on carbon coated copper grid, air-dried and employed for imaging purpose.

2.2.4. Dynamic light scattering (DLS) and zeta potential

DLS and zeta potential measurements were performed using a Beckman Coulter Delsa Nano C equipment. It may be mentioned here that BSA itself has a hydrodynamic diameter around 7 nm [31]. However, the scattering from BSA in absence of Ag-NP was found to be insignificant compared to that from NP. DLS measurements were performed with the as prepared dispersions. Zeta potential measurements were performed at different pH values in the 2.5–10.5 range. In the control experiment with BSA alone no measurable zeta potential was possible at the maximum concentration of the protein (100 μM).

2.2.5. Colloidal stability studies

To study the colloidal stability of Ag-NP in media of high ionic strength, 1 mL of Ag-NP dispersion was diluted with different volumes of $NaNO_3$ or MHB in order to reach different ionic concentrations (between 0.2 M and 1.15 M). All the spectra were corrected by dilution.

2.2.6. Surface enhanced Raman spectroscopy (SERS)

The SERS spectra were obtained with a Horiba – Jobin Yvon spectrometer (LABRAM-HR). A liquid-nitrogen-cooled charge coupled device (CCD) detector (Jobin Yvon, model CCD3000) was used in these measurements. A spectral resolution of 1 cm^{-1} was used. The 632 nm line of a He/Ne laser was used as the excitation sources in

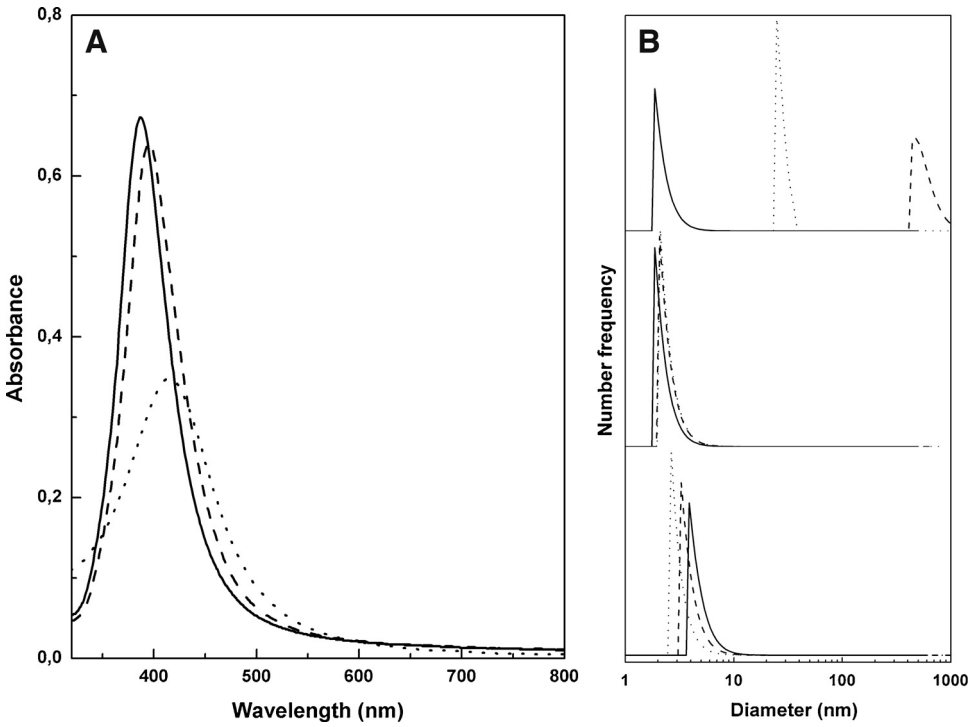

Fig. 1. (A) UV–vis spectra of Ag-NP/citrate (solid line), Ag-NP/BSA1 (dashed line) and Ag-NP/BSA2 (dotted line). (B) Size distribution of Ag-NP/citrate (top), Ag-NP/BSA1 (middle) and Ag-NP/BSA2 (bottom) dispersed in the reaction medium (solid line), in 0.20 M (top) or 1.15 M (middle and bottom) $NaNO_3$ (dashed) and MHB (dotted line).

the 200–1500 cm^{-1} range. The laser power at the sample was set at 3.5 mW. Special care was taken to monitor whether the laser power damaged the sample. The original spectra were smoothed using the Savitsky–Golay 5 points smoothing procedure.

2.2.7. Antimicrobial activity

To determine the minimum inhibitory concentration (MIC) and the minimum bactericidal concentration (MBC) of Ag-NP (freshly prepared and reconstituted in water after 6 months of storage in powder form) and Ag^+ ions, the procedure described by P. Sanpui et al. [32] was followed. Briefly, an overnight culture of *S. aureus* or *S. epidermidis* was inoculated into MHB medium supplemented with different concentrations of Ag-NP or Ag^+ ions and grown overnight at 37 °C. The bacterial concentration was 10^3 CFU/mL. The minimum concentration of the Ag-NP or Ag^+ ions which gave cultures that did not become turbid was taken to be the MIC. The cultures that were not turbid were reinoculated in Mueller Hinton Agar and incubated overnight at 37 °C. The minimum concentration of Ag-NP or Ag^+ ions in the initial cultures that gave cultures that did not grow when reinoculated into Mueller Hinton Agar was taken to be the MBC. All the experiments were realized by triplicate.

These experiments were also carried out with commercially available bone cement and bone substitute loaded with Ag-NP/BSA2. In this last case, the antimicrobial activity was also checked from the amount of Ag^+ ions released to the medium by potentiometry using H_2O_2 to assure the complete oxidation of Ag-NP.

3. Results

3.1. Synthesis and characterization of Ag-NP

Ag-NP were synthesized using three different methods based on the reduction of Ag^+ ions by $NaBH_4$: (1) the well-known citrate procedure (Ag-NP/citrate); (2) adding BSA after the reduction step (Ag-NP/BSA1); and (3) adding BSA before the reduction step (Ag-NP/BSA2). It has been well documented [14] that citrate ions act as a capping agent to prevent Ag-NP aggregation. Further, BSA added after the reduction step was already studied regarding the protein–NP interactions and their consequences on the particle size [20] and colloidal stability [14]. On the other hand, protein addition before the reduction step was performed with keratin as the stabilizing agent [19]. The used strategies are simple (mixing the reactants at room temperature), reproducible and low-cost.

Fig. 1A shows the UV–vis spectra of the three samples which are characterized by a single and intense peak corresponding to the Ag-NP surface plasmon resonance (SPR) band at around 400 nm [19]. Broadening and red-shifting of the SPR bands are observed for Ag-NP/BSA1 and Ag-NP/BSA2 compared to Ag-NP/citrate (see Table 1). Ag-NP/BSA2 SPR band presents a more significant broadening together with a stronger decrease in the intensity. Broadening, red-shifting and lower intensity of the SPR bands were also observed with other proteins added to the Ag-NP synthesis medium after the reduction step [20] and with keratin added before the reduction step [19]. TEM images (Supplementary information, Fig. S1) reveal individual entities for Ag-NP/BSA1 whereas NP dispersed in a protein matrix for Ag-NP/BSA2. Fig. 1B shows the number particle size distribution of Ag-NP/citrate, Ag-NP/BSA1 and Ag-NP/BSA2 obtained by DLS (see Supplementary information for the intensity particle size distributions, Fig. S2). The median hydrodynamic diameter of Ag-NP/citrate and Ag-NP/BSA1 is about 2 nm, while this value increases up to 4 nm for Ag-NP/BSA2. These values are in agreement with those reported in the literature for Ag-NP prepared in the absence and presence of proteins [19,20]. Ag-NP smaller than 10 nm are desirable to favor antimicrobial activity and nontoxic effect [33].

Fig. 2 shows zeta potential as a function of the pH for the different samples. For Ag-NP/citrate, the particles are negatively charged at pH higher than 4, with a nearly constant value at around −20 mV. Particle aggregation hampers zeta potential determinations at lower pH values due to the partial neutralization of the citrate ions which caused the flocculation of the aggregates.

Table 1
SPR band parameters of Ag-NP dispersed in different reaction media (as prepared), $NaNO_3$ solution, MHB and reconstituted (6 months storage) in water after freeze-drying.

SPR band	Ag-NP/citrate			Ag-NP/BSA1			Ag-NP/BSA2			
	As prepared	0.20 M $NaNO_3$	MHB	As prepared	1.15 M $NaNO_3$	MHB	As prepared	1.15 M $NaNO_3$	MHB	Reconstituted
Maximum (nm)	387	402 (510sh)	403 (sh)	395	395	398	415	415	406	419
Half width (nm)	59	98	230	65	74	133	108	117	ND	108

sh: shoulder; ND: non-determined.

This process also produces a diminution of the SPR band intensity together with an increment in the absorbance at higher wavelength values (Fig. S3). Ag-NP/BSA1 and Ag-NP/BSA2 samples show completely different behaviors compared to Ag-NP/citrate. The zeta potential values strongly depend on the pH, showing negative charge at pH higher than 5 and positive charge at lower pH. The isoelectric point (IEP) of Ag-NP/BSA1 and Ag-NP/BSA2 coincides with that of BSA-coated gold and silver nanoparticles [34] and BSA itself [14,35]. On the other hand, both samples present differences in the colloidal stability as a function of the pH. For Ag-NP/BSA1 a decrease of the intensity of the SPR band and an intense increase in a shoulder at 500 nm (Fig. S3) indicates a diminution in the colloidal stability at pH = IEP. This process is reverted by lowering the pH. On the other hand, the colloidal stability of Ag-NP/BSA2 is kept constant in the whole pH range (Fig. S3). BSA molecules strongly interact with NP surface and therefore, stabilize them particularly when BSA is added before the reduction step.

3.2. BSA–Ag-NP interactions

Fig. 3 shows the SERS spectra of native BSA, Ag-NP/BSA1 and Ag-NP/BSA2. The bands of these spectra can be divided into three groups corresponding to: sulfide containing bonds (S—S, S—C, S—Ag), secondary structure (C—C, C—N) and aromatic residues, such as tryptophan (Trp), tyrosine (Tyr) and phenylalanine (Phe), related to the tertiary structure. The spectrum of native BSA displays the characteristic vibration of S—S bond around 500 cm^{-1} arising from the multiple disulfide bonds in the protein [36]. In the presence of Ag-NP, a new band at 250 cm^{-1} appears due to the Ag—S bond [37] and the S—S band shifts to lower wavenumbers [37,38]. Moreover, other two new bands are present in the spectrum of Ag-NP/BSA2 at 632 and 694 cm^{-1} assigned to the S—C bond [39]. The characteristic vibrations of the second group are observed in the three spectra at 960 (native BSA) and 930 (Ag-NP) cm^{-1} due to the C—C bond and at 1240 cm^{-1} corresponding to the amida III band. These vibrations are related to α-helix secondary structure [37,38]. Finally, native BSA shows the characteristic vibrations of Trp (750 and 1340 cm^{-1}), Tyr (860 cm^{-1}) and Phe (1000 cm^{-1}) residues [38,39]. These bands are shifted, split and enhanced in the presence of Ag-NP, in agreement with the ability of Ag-NP to quench the intrinsic fluorescence of BSA [40]. These spectral features indicate that disulfide bonds are cleaved to form new ones with the surface of the nanoparticle, which partially modifies the tertiary structure around Trp, Tyr and Phe residues while the secondary structure is marginally altered. It is worth mentioning that some spectral features depend on the stage of the synthesis in which the protein is added to the reaction medium. The spectrum of Ag-NP/BSA1 shows more intense bands in the third group (tertiary structure) whereas Ag-NP/BSA2 one displays new bands related to the sulfide bonds. Enhanced bands are due to the surface effect produced by the Ag-NP suggesting that Trp, Tyr and Phe residues are closer to the Ag surface in Ag-NP/BSA1. On the other hand, the effect on the protein conformation is more severe when BSA is added before the reduction step, mainly affecting the multiple disulfide bonds of the protein.

3.3. Colloidal stability of Ag-NP in biologically relevant conditions

Figs. 1B and 4 compare the number particle size distribution and the UV–vis spectra, respectively, of the three samples dispersed in $NaNO_3$ or MHB at pH 8.0. The increase in the hydrodynamic diameter of the Ag-NP/citrate (Fig. 1B, top) and the diminution of the SPR band intensity together with the presence of a shoulder at 600 nm (Table 1) indicate that a 0.20 M $NaNO_3$ solution induces the NP aggregation. This behavior was observed in the whole range

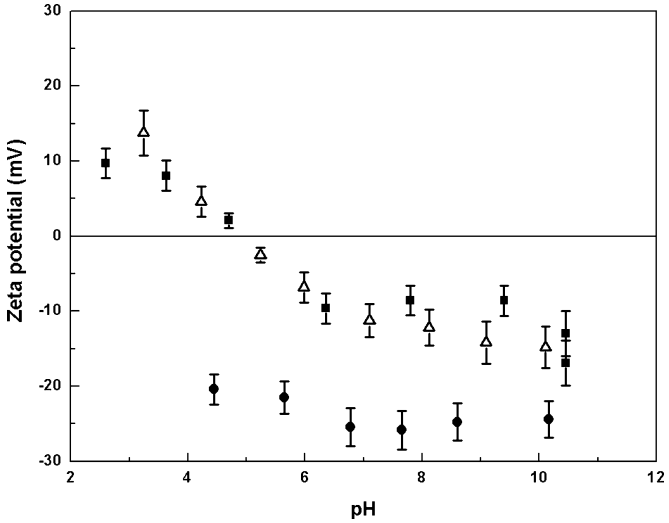

Fig. 2. Zeta potential as a function of the pH of Ag-NP/citrate (circles), Ag-NP/BSA1 (triangles) and Ag-NP/BSA2 (squares).

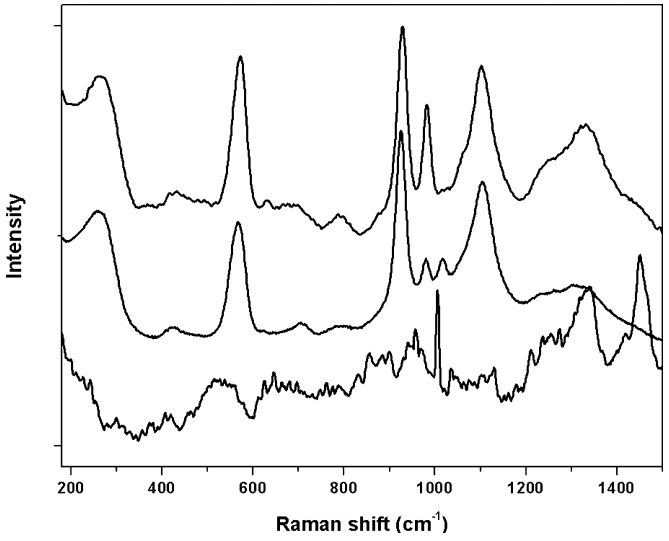

Fig. 3. SERS spectra for native BSA (bottom), Ag-NP/BSA1 (middle) and Ag-NP/BSA2 (top) in powder form. Conditions for the spectra: 632 nm excitation, 10 s integration × 10 accumulations.

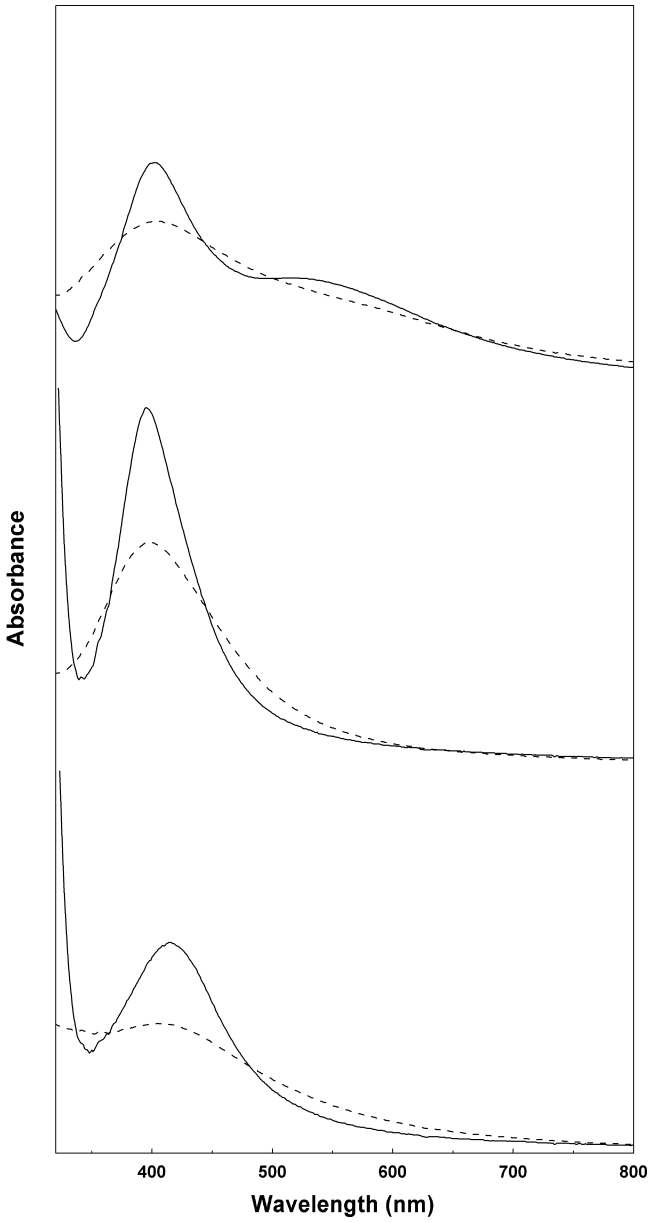

Fig. 4. UV–vis spectra of Ag-NP dispersed in $NaNO_3$ and MHB solutions. Top: Ag-NP/citrate dispersed in 0.20 M $NaNO_3$ (solid line) and in MHB (dashed line). Middle: Ag-NP/BSA1 and bottom: Ag-NP/BSA2 dispersed in 1.15 M $NaNO_3$ (solid line) and in MHB (dashed line).

of $NaNO_3$ concentration studied (0.20–0.85 M) as well as in MHB. These results do not agree with the reported behavior of commercially available 20 nm Ag-NP, suggesting that the NP size plays a role in determining the stability at high ionic concentration [41]. The unchanged NP diameter and SPR spectra clearly indicate that BSA stabilizes Ag-NP even in the presence of higher ionic concentrations than physiologic conditions. It is important to note that the spectral changes caused by MHB are due to modifications in the optical properties of the dispersant medium, since NP aggregation is discarded from both macroscopically visual inspection and DLS measurements in a wide diameter range. These results further emphasize that BSA enhances the stability of Ag-NP in media with high ionic strength. Moreover, the colloidal stability conferred by BSA to the NP enables studying the antimicrobial properties while the lack of stability of Ag-NP/citrate dispersed in MHB hampers this determination.

Table 2
MIC and MBC values of BSA stabilized Ag-NP and Ag^+ ions (μM), freshly prepared and after 6 months of storage in powder form and reconstituted in water.

	Ag-NP/BSA1	Ag-NP/BSA2		Ag^+ ions
	As prepared	As prepared	Reconstituted	
S. aureus	2	0.1	0.1	200
S. epidermidis	1	0.1	0.1	200

3.4. Antimicrobial activity of BSA stabilized Ag-NP

Table 2 compares the MIC and MBC values of BSA stabilized Ag-NP and Ag^+ ions, indicating that the presence of BSA does not prevent antimicrobial activity. The concentration values for Ag-NP were calculated assuming that 100% of the added Ag^+ ions reacted to form spherical Ag-NP (2 and 4 nm diameter of Ag-NP/BSA1 and Ag-NP/BSA2, respectively) during the reduction reaction [23]. Both Ag-NP and Ag^+ show bactericidal behavior (MIC = MBC) against *S. aureus* and *S. epidermidis* which is more effective with BSA stabilized NP (the NP concentration is 100–1000 times lower than the ions concentration). *S. aureus* and *S. epidermidis* seem to be more susceptible to Ag-NP/BSA2 than Ag-NP/BSA1, since a lower concentration of the first sample is necessary to reach the bactericidal effect.

It has already been reported a change from micromolar to nanomolar concentrations when comparing the bactericidal effect of Ag^+ ions to Ag-NP (smaller than 10 nm) [1]. On the other hand, Ag-NP prepared through an organometallic method tested against *E. coli*, *S. aureus* and *L. monocytogenes* leaded to MIC and MBC values between 12.5 and 25 $\mu g\,mL^{-1}$ [42]. Therefore, BSA stabilized Ag-NP are indeed extremely efficient as antimicrobial agents. *In vitro* cytotoxicity studies showed that 65 nm Ag-NP appeared to be harmful for human osteoarthritic chondrocytes only at high concentrations (160–250 μM) [10]. On the contrary, antibacterial effects of polyvinylpyrrolidone (PVP) stabilized Ag-NP against *S. epidermidis* occurred at higher concentrations than those inducing cytotoxicity in primary osteoblasts and osteoclasts [11]. Finally, BSA stabilized Ag-NP were freeze-dried and stored as powders for at least six months and reconstituted in deionized water. These processes did not cause any change in the colloidal stability, particle size distribution and antimicrobial properties as indicated in Table 1 (see also Supplementary information, Fig. S4). As a matter of fact, powdered Ag-NP were incorporated into commercially

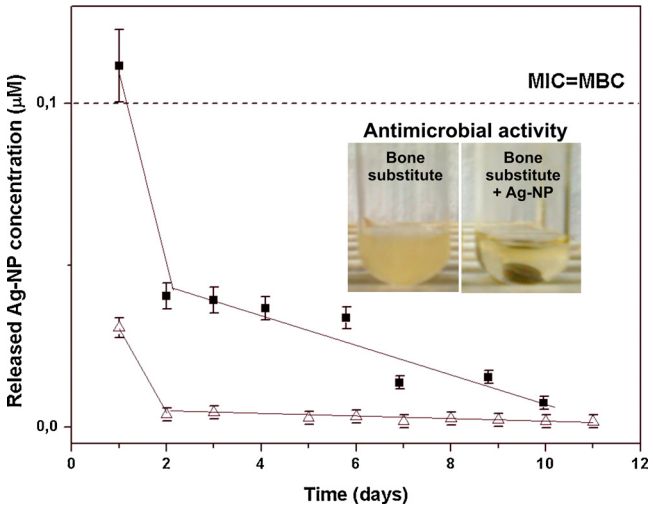

Fig. 5. Release profile of Ag-NP from bone cement (triangles) and bone substitute (squares). The inset shows the antimicrobial activity against *Staphylococcus aureus* by bone substitute in the presence and absence of Ag-NP incubated for 24 h.

available bone cement and bone substitute as antimicrobial additives. Fig. 5 shows the release profile for both biomaterials together with the antimicrobial activity. Ag-NP released from the cement was lower than the CIM while it was higher for the substitute during the first day. The observed difference may be due to the structural properties (hydrophobicity, porosity, roughness, *etc.*) of each one of the biomaterials. The release profile suggested a surface-controlled mechanism of Ag-NP from bone substitute [43]. Therefore, the proposed methods to stabilize Ag-NP not only produce stable dispersions in media of biological relevance but also long-lasting powders with appropriate antimicrobial activity when incorporated to biomaterials.

4. Discussion

The SPR band intensity depends on the surface morphology, size of the NP, dielectric environment and the refractive index of the medium [19,20]. Interaction of protein at the metal–water interface changes the local refractive index and dielectric properties and, therefore, SPR signal results as a sensitive measure of the protein–NP interaction [20]. The changes in the SPR band observed for both BSA stabilized Ag-NP, clearly indicate that these differences are due to the interaction between the protein molecules and the NP. Moreover, the SERS band at 250 cm^{-1} evidences the formation of Ag—S bonds in the presence of the protein. However, TEM, SERS and zeta potential results show that the properties of Ag-NP, the stabilization mode and the colloidal stability depend on the stage of the synthesis in which the protein is added to the reaction medium. These different behaviors can be traced from the interactions between BSA and Ag-NP caused by each one of the synthesis route. When the protein is added after the reduction step (Ag-NP/BSA1), these interactions mostly produce changes around the Trp, Tyr and Phe residues which are in the vicinity of the NP surface. Ag-NP/BSA1 are prepared in two steps, the first one involves the Ag-NP/citrate crystallization mechanism, followed by the exchange between the capping citrate anions and the protein molecules. Anchored BSA molecules stabilize individual NP, which strongly modifies the electrokinetic behavior of the Ag-NP. In this case, the stabilization is mainly electrostatic as it depends on the protein charge in agreement with the reported BSA adsorption mechanism at intermediate protein/Ag-NP ratio [20].

On the other hand, when BSA is added before the reduction step (Ag-NP/BSA2), the NP are formed in the presence of the protein molecules that undergo a severe change, especially in the disulfide motif of native BSA. Ag-NP formation in the presence of a protein stabilizer has been modeled with a recognition-reduction mechanism [19,44] in which the Ag^+ ions electrostatically attached to the protein backbone are reduced to form Ag nuclei together with the cleavage of some disulfide bonds. This mechanism may also apply with BSA stabilized Ag-NP that exhibit a high colloidal stability even at the IEP. Hence, the perturbed conformation of the protein causes Ag-NP to be remarkably well stabilized by the BSA matrix.

Regarding to the colloidal stability of Ag-NP, the differences are evident when comparing citrate and BSA coated NP. When surface molecules stabilizing the Ag-NP provide colloidal stability only through electrostatic means, as in the case of citrate, the electrolyte concentration at biologically relevant conditions leads to rapid aggregation of the NP. When bulky ligands are employed instead, as in the case of BSA, the added contribution from steric repulsion increases the colloidal stability in biologically relevant electrolyte concentrations. BSA imparts colloidal stability to Ag-NP by both electrostatic (depending on the pH) and steric interactions. However, the stability provided by steric interactions is more evident for Ag-NP/BSA2 since the dispersion remains stable even at the IEP. Therefore, electrostatic repulsion from BSA partially contributes to the colloidal stability mechanism when BSA exchanges previously capping citrate ions. This effect determines the pH conditions at which Ag-NP/BSA1 can be used as antimicrobial agent. According to ASTM (American Society for Testing and Materials) standard for stability of colloidal suspension, a positive or negative zeta potential between 30 and 40 mV is indicative of a substance with moderate stability while absolute values above 40 mV are associated to high stability [45]. However, the colloidal stability of Ag-NP/BSA2 presents an extra contribution given by the steric repulsion which results in stable suspensions at lower zeta potential values (even at the IEP).

Considering that Ag-NP smaller than 10 nm can interact better with bacteria [11], the pronounced antimicrobial effect of Ag-NP/BSA1 and Ag-NP/BSA2 may be related to the narrow size distribution combined with the small particle size. If diffusion of Ag-NP into the inner side of the bacteria is indeed helpful, smaller NP with higher surface areas will have an advantage [19]. In the particular case of the activity against *S. aureus* and *S. epidermidis*, Ag-NP may be added to the biomaterials used as implants and prosthesis to produce a local effect to control orthopedic post-surgery infections. On this regard, the little amount of BSA stabilized Ag-NP needed to reach bactericidal effect is a great advantage to minimize any other toxic effect. In fact, the nanomolar level reached with Ag-NP/BSA2 is much lower than the cytotoxic dose determined *in vitro* on osteoblasts, osteoclasts and osteoarthritic chondrocytes [10,11]. Hence, the application of Ag-NP/BSA2 to medical implants may be nonhazardous to human health. Finally, the possibility of drying BSA stabilized NP as stable powders with the ability to be reconstituted without changing the stability and antimicrobial properties is also of great importance. In fact, the solid can be incorporated as additive of biomaterials or pharmaceutical products to confer antimicrobial activity in a powdered form in different formulations, dispersed in aqueous and non-aqueous solutions or coated on the surface of materials [23].

5. Conclusions

Antimicrobial activity can only be attained with strongly stabilized Ag-NP to be successfully employed in contact with medium of high ionic strength, as culture and extracellular media. BSA behaves as an excellent stabilizing agent when used during the NP synthesis or just after it. The different modes of Ag-NP stabilization by the action of BSA determine the nature of the interaction with the NP, control the aggregation behavior of the NP in media of biologic relevance and determine the concentration required to achieve antibacterial action. BSA used during the NP synthesis produced extremely efficient antimicrobial agent with bactericidal effect in the nanomolar range. The powdered biocidal agent is stable under storage and versatile, as it can be used in different forms.

Acknowledgments

The authors acknowledge FonCyT, SeCyT-UNC, CONICET and Raomed S. A. for financial support and Laboratorio de Nanoscopía y Nanofotónica, INFIQC-CONICET/UNC, Servicio Nacional de Microscopía – MINCyT for the use of the Raman facilities. LEV thanks CONICET and Raomed S. A. for the fellowship.

Appendix A. Supplementary data

Supplementary data associated with this article can be found, in the online version, at http://dx.doi.org/10.1016/j.colsurfb.2015.05.002

References

[1] J. García-Barrasa, J. López-de-Luzuriaga, M. Monge, Cent. Eur. J. Chem. 9 (2011) 7.
[2] D.D. Evanoff, G. Chumanov, ChemPhysChem 6 (2005) 1221.
[3] P. Sanpui, A. Chattopadhyay, S.S. Ghosh, ACS Appl. Mater. Interfaces 3 (2011) 218.
[4] A.J. Huh, Y.J. Kwon, J. Controlled Release 156 (2011) 128.
[5] S.B. Goodman, Z. Yao, M. Keeney, F. Yang, Biomaterials 34 (2013) 3174.
[6] M.P. Sullivan, K.J. McHale, J. Parvizi, S. Mehta, Bone Joint J. 96-B (2014) 569.
[7] S. Taheri, A. Cavallaro, S.N. Christo, L.E. Smith, P. Majewski, M. Barton, J.D. Hayball, K. Vasilev, Biomaterials 35 (2014) 4601.
[8] V. Alt, T. Bechert, P. Steinrücke, M. Wagener, P. Seidel, E. Dingeldein, E. Domann, R. Schnettler, Biomaterials 25 (2004) 4383.
[9] J.a. Lyndon, B.J. Boyd, N. Birbilis, J. Controlled Release 179 (2014) 63.
[10] N.A. Pascarelli, E. Moretti, G. Terzuoli, A. Lamboglia, T. Renieri, A. Fioravanti, G. Collodel, J. Appl. Toxicol. 33 (2013) 1506.
[11] C.E. Albers, W. Hofstetter, K.A. Siebenrock, R. Landmann, F.M. Klenke, Nanotoxicology 7 (2013) 30.
[12] K. Bilberg, M.B. Hovgaard, F. Besenbacher, E. Baatrup, J. Toxicol. 2012 (2012).
[13] M.R. Reithofer, A. Lakshmanan, A.T.K. Ping, J.M. Chin, C.a.E. Hauser, Biomaterials 35 (2014) 7535.
[14] R.I. MacCuspie, J. Nanopart. Res. 13 (2011) 2893.
[15] X. Li, J. Zhang, W. Xu, H. Jia, X. Wang, B. Yang, B. Zhao, B. Li, Y. Ozaki, Langmuir 19 (2003) 4285.
[16] D.K. Bhui, H. Bar, P. Sarkar, G.P. Sahoo, S.P. De, A. Misra, J. Mol. Liq. 145 (2009) 33.
[17] M. Chen, L.-Y. Wang, J.-T. Han, J.-Y. Zhang, Z.-Y. Li, D.-J. Qian, J. Phys. Chem. B 110 (2006) 11224.
[18] W. Lesniak, A.U. Bielinska, K. Sun, K.W. Janczak, X. Shi, J.R. Baker, L.P. Balogh, Nano Lett. 5 (2005) 2123.
[19] J.J. Martin, J.M. Cardamone, P.L. Irwin, E.M. Brown, Colloids Surf. B (2011) 354.
[20] V. Banerjee, K.P. Das, Colloids Surf. B (2013) 71.
[21] A. Gebregeorgis, C. Bhan, O. Wilson, D. Raghavan, J. Colloid Interface Sci. 389 (2013) 31.
[22] C.D. Walkey, J.B. Olsen, F. Song, R. Liu, H. Guo, D.W.H. Olsen, Y. Cohen, A. Emili, W.C.W. Chan, ACS Nano 8 (2014) 2439.
[23] J.-T. Tai, C.-S. Lai, H.-C. Ho, Y.-S. Yeh, H.-F. Wang, R.-M. Ho, D.-H. Tsai, Langmuir 30 (2014) 12755.
[24] M.N. Martin, A.J. Allen, R.I. MacCuspie, V.A. Hackley, Langmuir 30 (2014) 11442.
[25] A. Ravindran, P. Chandran, S.S. Khan, Colloids Surf. B 105 (2013) 342.
[26] K.K. Goli, N. Gera, X. Liu, B.M. Rao, O.J. Rojas, J. Genzer, ACS Appl. Mater. Interfaces 5 (2013) 5298.
[27] J.M. Gorham, A.B. Rohlfing, K.a. Lippa, R.I. MacCuspie, A. Hemmati, R. David Holbrook, J. Nanopart. Res. 16 (2014) 2339.
[28] R.I. MacCuspie, A.J. Allen, M.N. Martin, V.a. Hackley, J. Nanopart. Res. 15 (2013) 1760.
[29] A.O. Elzoghby, W.M. Samy, N.a. Elgindy, J. Controlled Release 157 (2012) 168.
[30] C.N. Lok, C.M. Ho, R. Chen, Q.Y. He, W.Y. Yu, H. Sun, P.K.H. Tam, J.F. Chiu, C.M. Che, J. Biol. Inorg. Chem. 12 (2007) 527.
[31] D.C. Carter, J.X. Ho in, C.B. Anfinsen, J.T. Edsall, F.M. Richards, D.S. Eisenberg (Eds.), Advances in Protein Chemistry, vol. 45, Academic Press, 1994, p. 153 (Structure of Serum Albumin).
[32] P. Sanpui, A. Murugadoss, P.V.D. Prasad, S.S. Ghosh, A. Chattopadhyay, Int. J. Food Microbiol. 124 (2008) 142.
[33] N. Ayala-Núñez, H. Lara Villegas, L. del Carmen Ixtepan Turrent, C. Rodríguez Padilla, NanoBiotechnology 5 (2009) 2.
[34] S. Gautam, P. Dubey, M.N. Gupta, Colloids Surf., B (102) (2013) 879.
[35] S.H. Brewer, W.R. Glomm, M.C. Johnson, M.K. Knag, S. Franzen, Langmuir 21 (2005) 9303.
[36] J.L. Burt, C. Gutiérrez-Wing, M. Miki-Yoshida, M. José-Yacamán, Langmuir 20 (2004) 11778.
[37] D. Joshi, R.K. Soni, Appl. Phys. A 116 (2014) 635.
[38] D. Zhang, O. Neumann, H. Wang, V.M. Yuwono, A. Barhoumi, M. Perham, J.D. Hartgerink, P. Wittung-Stafshede, N.J. Halas, Nano Lett. 9 (2009) 666.
[39] L.-J. Xu, C. Zong, X.-S. Zheng, P. Hu, J.-M. Feng, B. Ren, Anal. Chem. 86 (2014) 2238.
[40] S. Roy, T.K. Das, J. Nanosci. Nanotechnol. 14 (2014) 4899.
[41] S.C. Sahu, S. Roy, J. Zheng, J.J. Yourick, R.L. Sprando, J. Appl. Toxicol. 34 (2014) 1200.
[42] E.J. Fernández, J. García-Barrasa, A. Laguna, J.M. López-de-Luzuriaga, M. Monge, C. Torres, Nanotechnology 19 (2008) 185602.
[43] H. van de Belt, D. Neut, D.R.A. Uges, W. Schenk, J.R. van Horn, H.C. van der Mei, H.J. Busscher, Biomaterials 21 (2000) 1981.
[44] S. Li, Y. Shen, A. Xie, X. Yu, L. Qiu, L. Zhang, Q. Zhang, Green Chem. 9 (2007) 852.
[45] K. Krishnamoorthy, M. Veerapandian, K. Yun, S.J. Kim, Carbon 53 (2013) 38.